# Vibration of a Translating Follower Cam with Different Profiles Undergoing an Angular Acceleration 角加速度下不同輪廓的平移從動件凸輪的振動

<sup>1</sup>Department of Aircraft Engineering, Air Force Institute of Technology

<sup>2</sup>Department of Aircraft Maintenance, Far East University

<sup>3</sup>Department of Mechanical Engineering, Air Force Institute of Technology

1空軍航空技術學院飛機工程系

2 遠東科技大學飛機修護系

3空軍航空技術學院機械工程科

#### **Abstract**

The purpose of this study is to investigate the transverse vibration of a translating follower cam with different cam profiles undergoing an angular acceleration. The follower is flexible and vibrates transversely. Four different motions are employed to design the rise and fall motion of the follower. They include modified sinusoidal acceleration motion, modified trapezoidal acceleration motion, 4-5-6-7 polynomial motion, and 3-4-5 polynomial motion. The contact position of the roller and the cam, which cannot be determined only by the kinematics analysis is formed as geometric constraints and substituted into the dynamics modeling. The governing system equations of motion by using Hamilton's principle and the assumed mode method can be derived. And Runge-Kutta method is employed to solve the vibration response of the translating follower. The numerical results show that the vibration response is affected significantly by the cam profiles. The response amplitude of the follower using modified sinusoidal acceleration motion and 3-4-5 polynomial motion are smaller and slower to increase than that using the other two methods.

Keywords: cam profile, angular acceleration, translating follower, transverse vibration, different profiles.

#### 摘要

本研究的目的是研究角加速度作用下具有不同凸輪輪廓的平移從動凸輪的橫向振動,從動件考慮為撓性而造成側向振動。四種不同運動用來設計從動件的上升與下降運動,包含有修正正弦加速度運動、修正梯形加速度運動、4-5-6-7多項式運動及3-4-5多項式運動。滾子與凸輪的接觸點,無法僅由運動學分析決定,將其考慮為幾何限制,並代入動力模擬。使用漢彌頓原理與假設模態法,可導出統御運動方程式,並以阮奇-庫達法求解平移從動件的振動響應。數值結果顯示振動響應受凸輪輪廓的顯著影響,採用修正正弦加速度運動和3-4-5多項式運動的從動件的響應振幅比使用其他兩種方法的響應振幅小且增加較慢。

關鍵字:凸輪輪廓,角加速度,平移式從動件,側向振動

#### 1. INTRODUCTION

Reference [1] introduces the related topics of cam-actuated mechanisms. Several studies have been reported on the kinematic analysis of cam mechanisms [2]. Some researchers have also investigated the dynamics of cam mechanisms. Chang et al. [3] studied the lateral vibration of a translational roller follower cam due to a flexible follower rod. Cycloidal profile was used to design the rise and fall intervals of the follower's rise-dwell-fall-dwell motion. The numerical results showed that follower rod with longer length or smaller cross-sectional radius caused larger follower response amplitude. Smaller cam base-circle radius or larger total lift also resulted in a larger response.

Hejma et al. [4] studied a mechanism configuration consisting of a flat faced follower pressed against the surface of a radial cam by a coil spring. On the basis of known lifting function, a new cam profile was proposed. The lifting function a polynomial character. In particular, polynomial of degree 3, 5 and 7 were studied. A method was proposed to calculate the torque from the desired cam angular velocity. This method was used to select a suitable motor and correctly select a coil spring. The spring preload was determined to avoid the follower bouncing off the cam surface. Based on the analytical analysis, a new measuring bench was proposed. Yousuf [5] studied the influence of the inner distance of the guide rail, the constant speed of the cam and the offset of the follower on the chaotic phenomenon. The chaotic phenomena was investigated using Phase-plane portrait with Poincare' maps, power density function of Fast Fourier Transform (FFT), and largest Lyapunov exponent. The chaos analysis of the offset flat-faced follower due to the contact with the polydyne cam profile was controlled using multi linear and nonlinear damper systems. The suspensions of the shocks absorbers were described using spring-damper-mass systems. The nonlinear response of the flat-faced follower due to the offset shift was calculated at different internal distance of the follower guide, different speeds of the cam, and different followers' offsets.

In this paper, following the same approach of the previous study [3], one can study the follower vibration of a translating follower cam system with four cam profiles undergoing an angular acceleration. Four motions including modified sinusoidal acceleration motion, modified trapezoidal acceleration motion, 4-5-6-7 polynomial motion, and 3-4-5 polynomial motion will be considered to design the rise and fall portions of the rise-dwell-fall-dwell (RDFD) motion of the follower. The vibration under the four profiles will be calculated and discussed.

#### 2. FOUR RDFD MOTION

Figure 1 shows the schematic diagram of a translating follower cam.  $S(\theta)$  represents the follower displacement function and  $\theta$  is the cam rotating angle. Figure shows the rise-dwell-fall-dwell (RDFD) motion the translating follower. The rise interval of the translating follower is  $0 \text{ rad} \le \theta \le \beta \text{ rad}$  and the fall interval is  $\pi \ rad \le \theta \le \pi + \beta \ rad$ . The value of  $\beta$  is given as  $\pi/2$  in this study. Four rise and motions such modified sinusoidal acceleration modified motion, trapezoidal acceleration motion, 4-5-6-7 polynomial motion, and 3-4-5 polynomial motion are applied to design

the cam profile. The displacement function  $S(\theta)$  for the rise segment is given below: (Chen [1])

1. Modified sinusoidal acceleration motion:

$$0 \le \theta \le \frac{\beta}{8}$$
:

$$S(\theta) = S_T \left( \frac{\pi}{4 + \pi} \frac{\theta}{\beta} - \frac{\pi}{4(4 + \pi)} \sin(\frac{4\pi\theta}{\beta}) \right)$$
 (1.1)

$$\frac{\beta}{8} < \theta \le \frac{7\beta}{8}$$
:

$$S(\theta) = S_T \left( \frac{2}{4+\pi} + \frac{\pi}{4+\pi} \frac{\theta}{\beta} - \frac{9}{4(4+\pi)} \cos(\frac{4\pi\theta}{3\beta} - \frac{\pi}{6}) \right) (1.2)$$

$$\frac{7\beta}{8} < \theta \le \beta$$
:

$$S(\theta) = S_T \left( \frac{4}{4+\pi} + \frac{\pi}{4+\pi} \frac{\theta}{\beta} - \frac{9}{4(4+\pi)} \sin(\frac{4\pi\theta}{\beta}) \right)$$
 (1.3)

2. Modified trapezoidal acceleration motion:

$$0 \le \theta \le \frac{\beta}{8}$$
:

$$S(\theta) = S_T \left( 0.38898448 \frac{\theta}{\beta} - 0.0309544 \sin(\frac{4\pi\theta}{\beta}) \right) (2.1)$$

$$\frac{\beta}{8} < \theta \le \frac{3\beta}{8}$$
:

$$S(\theta) = S_T \left( 2.44406 \left( \frac{\theta}{\beta} \right)^2 - 0.22203097 \frac{\theta}{\beta} + 0.00723407 \right)$$
(2.2)

$$\frac{3\beta}{8} < \theta \le \frac{\beta}{2}$$
:

$$S(\theta) = S_T \left( 1.6110154 \frac{\theta}{\beta} - 0.0309533 \sin(\frac{4\pi\theta}{\beta} - \pi) - 0.3055077 \right)$$
(2.3)

$$\frac{\beta}{2} < \theta \le \frac{5\beta}{8}$$
:

$$S(\theta) = S_T \left( 1.6110154 \frac{\theta}{\beta} + 0.0309544 \sin(\frac{4\pi\theta}{\beta}) - 0.3055077 \right)$$
(2.4)

$$\frac{5\beta}{8} < \theta \le \frac{7\beta}{8}$$
:

$$S(\theta) = S_T \left( -2.44406184 \left( \frac{\theta}{\beta} \right)^2 + 4.6660917 \frac{\theta}{\beta} - 1.2292648 \right)$$
(2.5)

$$\frac{7\beta}{8} < \theta \le \beta$$
:

$$S(\theta) = S_T \left( 0.6110154 + 0.38898448 \frac{\theta}{\beta} + 0.0309544 \sin(\frac{4\pi\theta}{\beta} - \pi) \right)$$
(2.6)

3. 4-5-6-7 polynomial motion:

 $0 \le \theta \le \beta$ :

$$S(\theta) = S_T \left( 35 \left( \frac{\theta}{\beta} \right)^4 - 84 \left( \frac{\theta}{\beta} \right)^5 + 70 \left( \frac{\theta}{\beta} \right)^6 - 20 \left( \frac{\theta}{\beta} \right)^7 \right)$$
 (3)

4. 3-4-5 polynomial motion:

 $0 \le \theta \le \beta$ :

$$S(\theta) = S_T \left( 10 \left( \frac{\theta}{\beta} \right)^3 - 15 \left( \frac{\theta}{\beta} \right)^4 + 6 \left( \frac{\theta}{\beta} \right)^5 \right) \tag{4}$$

In Equtions (1)-(4),  $\beta$  and  $S_T$  represent the period of the rise and fall segments and the total lift magnitude, respectively. The above four motions are used directly for the rise portion of the cam. The fall displacement can also be derived by subtracting the rise displacement function  $S(\theta)$  from the maximum lift  $S_T$ .

## 3. DERIVATION OF GOVERING EQUATIONS

Following the same approach of the previous study [3], the follower vibration of a disk cam system with different profiles undergoing an angular acceleration will be investigated in this study. Figure 1 shows a disk cam with a translating roller follower (same system as [3]). The cam is assumed to be rigid and the roller is pinned to the follower which is considered to be flexible and described by using Rayleigh beam theory. By using the theory of

envelopes (Chen [1]), the cam profile can be determined. The profile coordinates  $(x_{1C}, y_{1C})$  are derived as follows (refer to Fig. 1):

$$x_{1C} = r\cos\theta - \frac{r_r Q}{\sqrt{P^2 + Q^2}},$$

$$y_{1C} = r\sin\theta + (x_{1C} - r\cos\theta)\frac{P}{Q}.$$
(5)

where

$$r = r_b + r_r + S(\theta),$$

$$P = r \sin \theta - S'(\theta) \cos \theta,$$

$$Q = r \cos \theta + S'(\theta) \sin \theta.$$
(6)

 $r_b$  is the base-circle radius of the cam,  $r_r$  is the roller radius and  $S(\theta)$  denotes the displacement function of the follower rod when the cam rotates an angle  $\theta$ . And the coordinates of the roller center E in Figure 1 are

$$x_{1E} = r\cos\theta, y_{1E} = r\sin\theta.$$
 (7)

A rotating frame  $O_1 - x_1 y_1$  fixed on the cam which rotates an angle  $\phi$  undergoing an angular acceleration is shown in Fig. 3. A fixed frame  $O_2 - xy$  is also used. The  $O_2x$  axis coincides with the centerline of the undeformed rod. The flexible follower undergoes a transverse deflection, v(x,t). The end point E moves to be E' after deformation. The transverse deflection at the end point E are denoted as  $v_E$ , i.e.,  $v_E = v(l,t)$ . A fixed frame  $O_1 - XY$  is also used. The fixed coordinates for the points C and E are given as follows:

$$X_{C} = x_{1C} \sin \phi - y_{1C} \cos \phi,$$

$$Y_{C} = x_{1C} \cos \phi + y_{1C} \sin \phi,$$

$$X_{E} = x_{1E} \sin \phi - y_{1E} \cos \phi,$$

$$Y_{E} = x_{1E} \cos \phi + y_{1E} \sin \phi.$$
(8)

where the angle  $\phi = \int_0^t \Omega(\tau) d\tau$ .  $\Omega$  represents the rotating speed of the cam and is time dependent.

From the geometric relationship shown in Fig. 3, two constraint equations of point E are deduced as

$$\Phi_1 = X_E - \nu_E = 0 \tag{9}$$

$$\Phi_2 = Y_E + x_E - d = 0 \tag{10}$$

The kinetic energy  $T_{rod}$  and the strain energy  $U_{rod}$  of the rod can be derived as

$$T_{rod} = \frac{1}{2} \int_0^{x_E} \rho A(\dot{x}^2 + \dot{v}^2) dx + \frac{1}{2} \int_0^{x_E} \rho I \dot{v}_{,x}^2 dx \quad (11)$$

$$U_{rod} = \frac{1}{2} \int_0^{x_E} E I v_{,xx}^2 dx$$
 (12)

where  $\rho$  is the mass density of the rod. A is the cross-sectional area of the rod. I is the area moment of inertia of the rod cross-section. E is Young's modulus of beam material.

The kinetic energy of the roller is derived as

$$T_{roller} = \frac{1}{2} m_r (\dot{X}_E^2 + \dot{Y}_E^2) + \frac{1}{2} \frac{J_r}{r_r^2} [(\dot{X}_C - \dot{X}_E)^2 + (\dot{Y}_C - \dot{Y}_E)^2]$$
(13)

where  $m_r$  and  $J_r$  are the mass and the polar mass moment of inertia of the roller, respectively.

For satisfying the geometric boundary conditions at the rigid cylinder end (the deflection and the slope vanish), one can expand the deflections by applying the assumed mode method as follows,

$$v(x(t),t) = \sum_{i=2}^{N} b_i(t)x(t)^i$$
 (14)

where  $x^{i}$  is the mode shape which is time

dependent since the follower is driven by the cam to lengthen or shorten.  $b_i(t)$  is the associated amplitudes for the transverse deflection.

Applying Hamilton's principle for the whole system, the variation equation is established as

$$\int_{t_1}^{t_2} \delta(T_{rod} + T_{roller} - U_{rod} + \lambda_1 \Phi_1 + \lambda_2 \Phi_2) dt = 0 \quad (15)$$

where  $T_{rod}$  and  $T_{roller}$  are the kinetic energy of the follower rod and the roller, respectively.  $U_{rod}$  is the strain energy of the follower rod.  $\lambda_1\Phi_1$  and  $\lambda_2\Phi_2$  are the works done by the constraint forces.

Substituting equation (14) into Hamilton's principle (15), one can obtain the system equation of motion. The equation is expressed as

$$\mathbf{M}(\mathbf{Q})\ddot{\mathbf{Q}} + \mathbf{N}(\mathbf{Q}, \dot{\mathbf{Q}}) + \mathbf{\Phi}_{\mathbf{Q}}^{T} \lambda = \mathbf{0}$$
 (16)

where M, N, and  $\lambda$  are mass matrix, nonlinear vector, and Lagrange multiplier, respectively. Q is the generalized coordinate vector and expressed as

$$\mathbf{Q} = [b_1 \quad b_2 \quad \cdots \quad b_N \quad x_E \quad \boldsymbol{\theta}]. \tag{17}$$

The two constraints expressed in equations (9) and (10) are combined as the following form:

$$\mathbf{\Phi}(\mathbf{Q}) = \begin{bmatrix} \Phi_1 & \Phi_2 \end{bmatrix}^T = \mathbf{0} \tag{18}$$

Using the partitioning method (Parviz [6]) and Runge-Kutta integration method, one can solve the vibration response of the flexible follower of a disk cam system with different cam profiles undergoing an angular acceleration.

### 4. NUMERICAL RESULTS AND DISCUSSIONS

An example is studied to investigate the vibration of the translating roller-follower cam with

the four cam profiles undergoing an angular acceleration. The transverse vibration response at the end point E of the follower with different cam profile is calculated. Four cam profiles are considered to form the different rise and fall motion. They include modified sinusoidal acceleration motion, modified trapezoidal acceleration motion, 4-5-6-7 polynomial motion, and 3-4-5 polynomial motion. The angular acceleration  $\alpha$  in this study is assumed to be constant, so the angular speed of the cam is given as

$$\Omega(t) = \Omega_0 + \alpha t \tag{19}$$

where  $\Omega_0$  is the initial angular speed of the cam.

The period of the rise and fall segment  $\beta$  is set to  $\frac{\pi}{2}$ . The total rise  $S_T$  is set to 15 mm. The cross section of the follower rod is a circle with  $r_f = 5 \text{ mm}$  . The associated area and area inertia cross-sectional  $A = 78.54 \text{ mm}^2$  and  $I = 490.87 \text{ mm}^4$ . The elastic modulus and the density of the follower are  $E = 2.1 \times 10^8$  kg/mm·s<sup>2</sup> and  $\rho = 7.8 \times 10^{-6}$  kg/mm<sup>3</sup>. The distance from the lower end of the rigid cylinder and the rotation center of the cam is d = 112 mm. The base-circle radius of the cam is  $r_b = 26 \text{ mm}$ . The radius, mass, and mass polar moment of inertia of the roller are  $r_r = 5 \text{ mm}$ ,  $m_r = 0.05 \text{ kg} \text{ and } J_r = 0.625 \text{ kg} \cdot \text{mm}^2.$ 

In the previous study ([3]), the numerical results nearly converge with N=3, so the assumed mode method with N=3 is applied in this study. The vibration response of the translating roller-follower cam with four cam profiles undergoing an angular acceleration is investigated. Three cases of angular accelerations including 10, 20, and 30  $rad/s^2$  are

studied. The initial angular speed is given as 240 rad/s. The transverse vibration responses of the output node E for the first five cam cycles are plotted. They are shown in Figures 4-15.

For the cam profile of the modified sinusoidal acceleration motion, Figures 4, 8, and 12 show the vibration response of the system at the angular acceleration of  $10 \ rad/s^2$ ,  $20 \ rad/s^2$ , and  $30 \ rad/s^2$ , respectively. When the angular acceleration gets larger, the vibration response becomes larger. The response gets large faster obviously as the cam undergoes a larger angular acceleration. The vibration responses are affected significantly by the cam rotational speed and angular acceleration. The response amplitude tends to increase as the rotational speed increases.

For the cam profile of the modified trapezoidal acceleration motion, Figures 5, 9, and 13 show the vibration response of the system at the angular acceleration of  $10 \text{ rad/s}^2$ ,  $20 \text{ rad/s}^2$ , and  $30 \, rad \, / \, s^2$ , respectively. For the cam profile of the 4-5-6-7 polynomial motion, Figures 6, 10, and 14 show the vibration response of the system at the angular acceleration of  $10 \, rad \, / \, s^2$ ,  $20 \, rad \, / \, s^2$ , and  $30 \, rad \, / \, s^2$ , respectively. For the cam profile of the 3-4-5 polynomial motion, Figures 7, 11, and 15 show the vibration response of the system at the angular acceleration of  $10 \, rad \, / \, s^2$ ,  $20 \, rad \, / \, s^2$ , and  $30 \, rad \, / \, s^2$ , respectively. The results by using the modified trapezoidal acceleration motion, the 4-5-6-7 polynomial motion, and the 3-4-5 polynomial motion are similar to those by using the modified sinusoidal acceleration motion. The vibration response becomes larger when the angular acceleration gets larger under the condition of the same motion. The response amplitude enlarges as

the angular speed increases. The response increase faster with increasing cam rotating angle and speed as the cam undergoes a larger angular acceleration. The cam rotational speed and angular acceleration affect significantly the vibration responses of the follower.

To compare the response amplitude of the follower, it is found from Figures 4-15 that the response for the first five cycles is smaller for the cam profile using the modified sinusoidal acceleration motion and the 3-4-5 polynomial motion. And the increase in response during the periods of the rise and fall using the modified sinusoidal acceleration motion and the 3-4-5 polynomial motion is slower than that using the other two methods. The response in the dwell intervals using the 3-4-5 polynomial motion increases slower than that using the other three methods.

#### 5. CONCLUSIONS

The equations of motion for the vibration of a translating roller-follower cam are derived by using Hamilton's principle and the assumed mode method. From the numerical studies, it is shown that the vibration responses are affected significantly by the cam profile. By using the same profile, the response amplitude enlarges as the angular speed increases. The response gets large faster obviously as the cam undergoes a larger angular acceleration. The response is smaller and slower to increase for the cam profile using the modified sinusoidal acceleration motion and the 3-4-5 polynomial motion. The response in the dwell intervals using the 3-4-5 polynomial motion increases slower than that using the other three methods.

#### REFERENCES

- Chen, F. Y., Mechanics and Design of Cam Mechanisms, Pergamon Press, New York, 1982.
- Borboni, A., Aggogeri, F., Elamvazuthi, I., Incerti G., and Magnani, P. L., 2020 "Effects of profile interpolation in cam mechanisms" Mechanism and Machine Theory, 144, 103625.
- Chang, J. R., Huang, C. J., Huang, M. C., Jou, B. H., and Hsu, H. P., 2018, "Transverse vibration analysis of a translating roller-follower cam using cycloidal profile for RDFD motion," Journal of Air Force Institute of Technology, 17, pp. 115-122.
- Hejma, P., Svoboda, M., Kampo, J., and Soukup, J., 2017, "Analytic analysis of a cam mechanism," Procedia Engineering, 177, pp. 3-10.
- Yousuf, L. S., 2022, "Nonlinear dynamics phenomenon detection in a polydyne cam with an offset flat-faced follower mechanism using multi shocks absorbers systems," Applications in Engineering Science, 9, 10008.
- Parviz, E. N., Computer-aided analysis of mechanical system, Prentice-Hall International Edition, 1988, pp. 46.

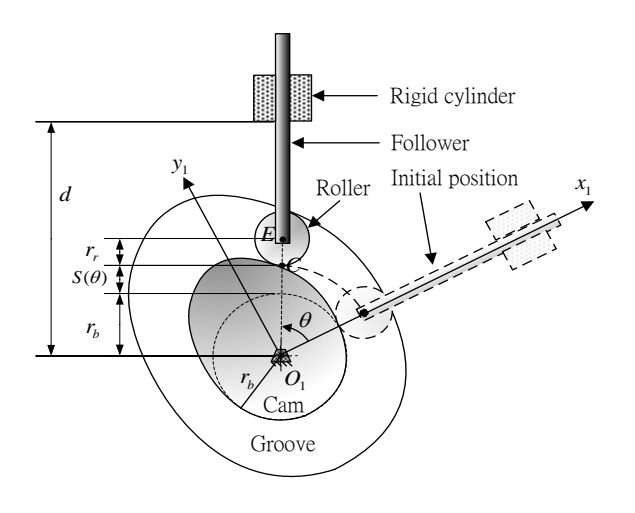


Fig. 1 Schematic of a translating follower cam.

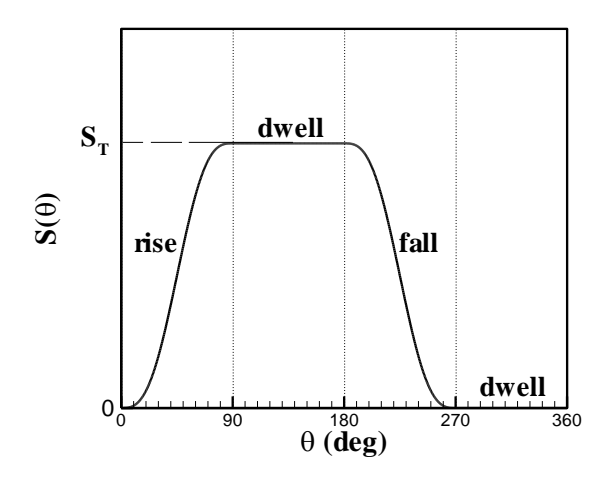


Fig. 2 The studied RDFD motion for  $\beta = \frac{\pi}{2} rad$ 

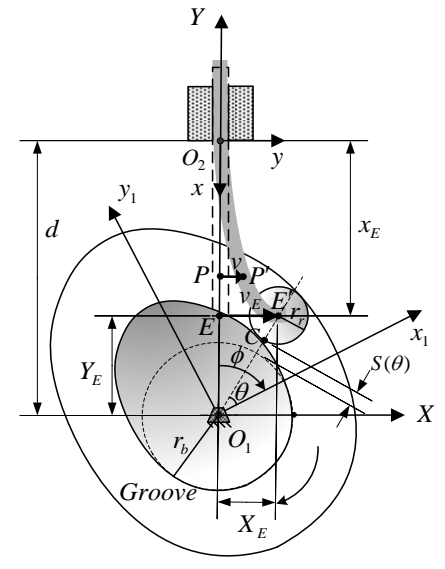


Fig. 3 Deformed configuration of the cam mechanism.

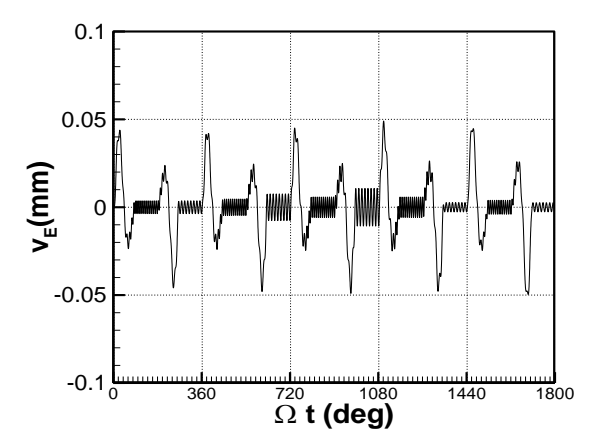


Figure 4 The vibration response  $v_E$  at  $\alpha = 10 \, rad \, / \, s^2$  with modified sinusoidal acceleration motion.

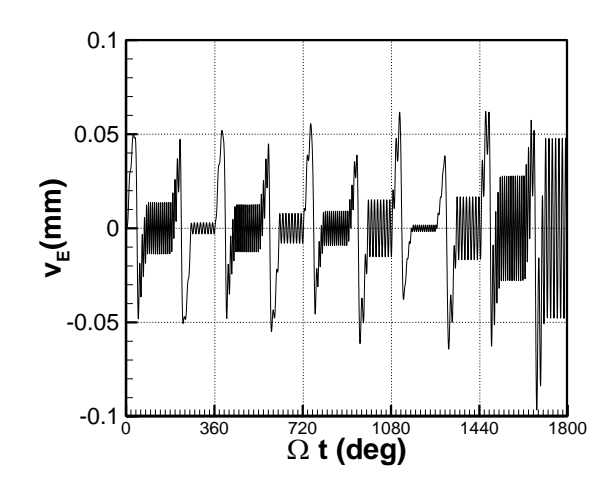


Figure 5 The vibration response  $v_E$  at  $\alpha = 10 \ rad \ / \ s^2$  with modified trapezoidal acceleration motion.

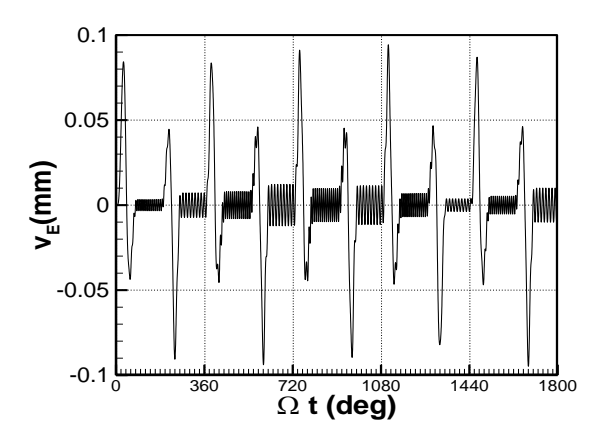


Figure 6 The vibration response  $v_E$  at  $\alpha = 10 \, rad \, / \, s^2$  with 4-5-6-7 polynomial motion.

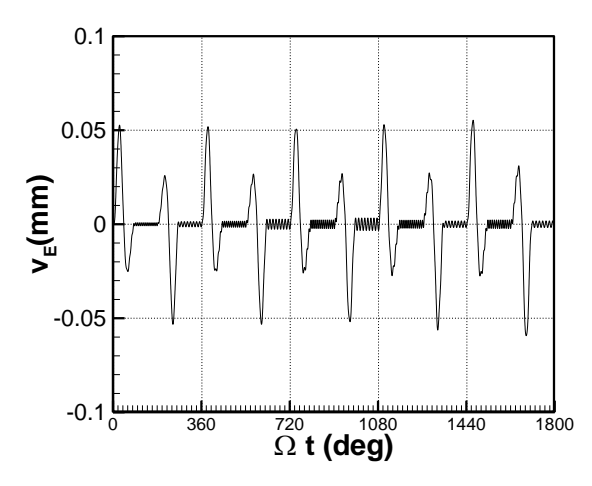


Figure 7 The vibration response  $v_E$  at  $\alpha = 10 \, rad \, / \, s^2$  with 3-4-5 polynomial motion.

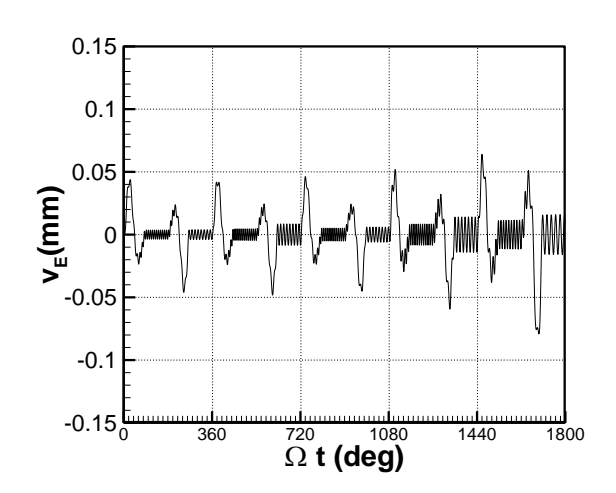


Figure 8 The vibration response  $v_E$  at  $\alpha = 20 \, rad \, / \, s^2$  with modified sinusoidal acceleration motion.

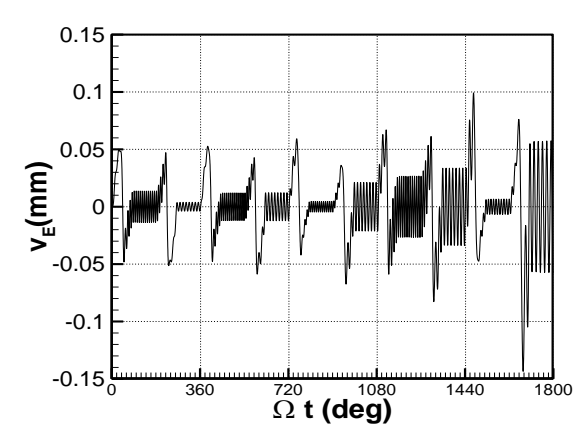


Figure 9 The vibration response  $v_E$  at  $\alpha = 20 \, rad \, / \, s^2$  with modified trapezoidal acceleration motion.

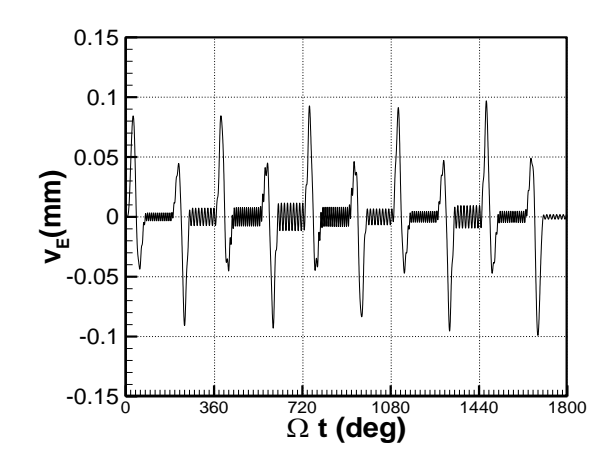


Figure 10 The vibration response  $v_E$  at  $\alpha = 20 \, rad / s^2$  with 4-5-6-7 polynomial motion.

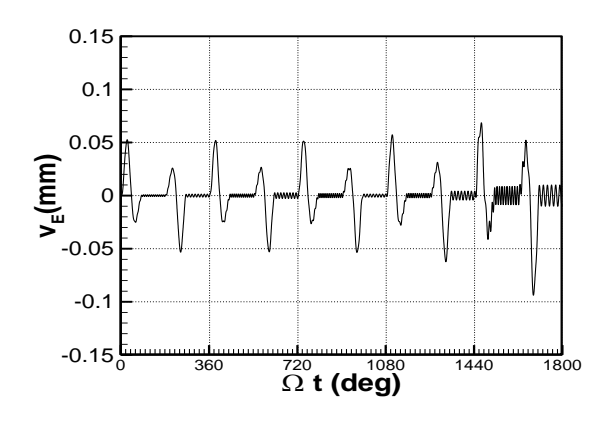


Figure 11 The vibration response  $v_E$  at  $\alpha = 20 \, rad \, / \, s^2$  with 3-4-5 polynomial motion.

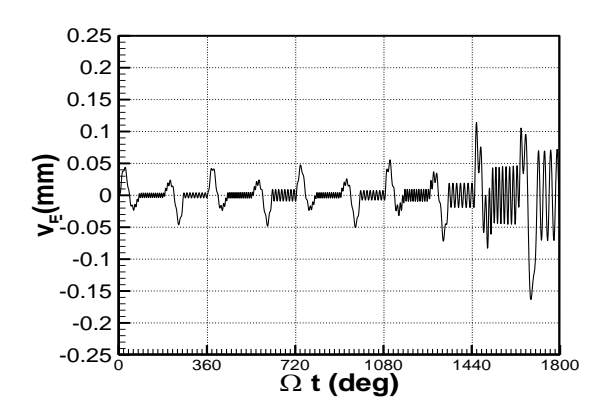


Figure 12 The vibration response  $v_E$  at  $\alpha = 30 \, rad \, / \, s^2$  with modified sinusoidal acceleration motion.

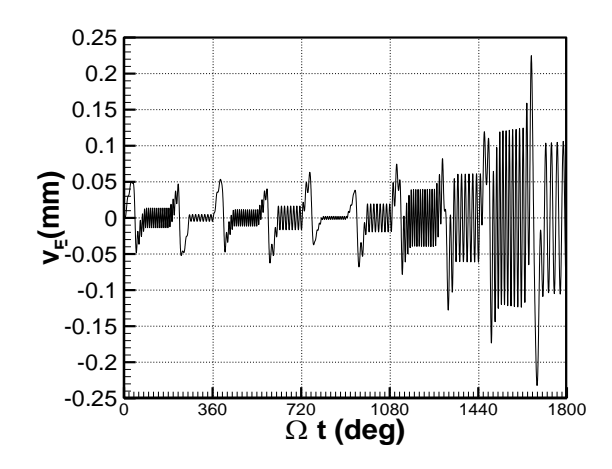


Figure 13 The vibration response  $v_E$  at  $\alpha = 30 \, rad \, / \, s^2$  with modified trapezoidal acceleration motion.

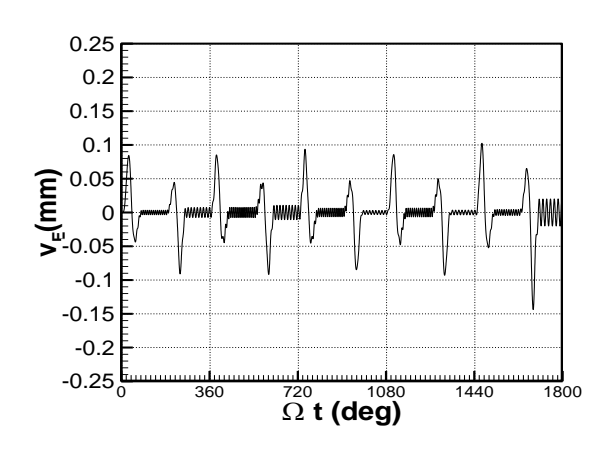


Figure 14 The vibration response  $v_E$  at  $\alpha = 30 \, rad / s^2$  with 4-5-6-7 polynomial motion.

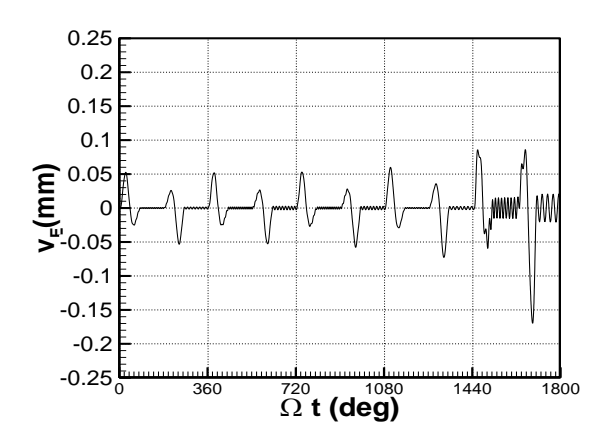


Figure 15 The vib ration response  $v_E$  at  $\alpha = 30 \, rad \, / \, s^2$  with 3-4-5 polynomial motion.

航空技術學院學報 第二十二卷 (民國一一二年)